INTERNATIONAL JOURNAL FOR NUMERICAL METHODS IN FLUIDS, VOL. 24, 1307–1319 (1997)

PREDICTING THE WIND NOISE FROM THE PANTOGRAPH COVER OF A TRAIN

BAYARD S. HOLMES,[1,*] JOÃO B. DIAS,[1,*] BELGACEM A. JAROUX,[2] TAKAMITSU SASSA[3] AND YASUHIRO BAN[3]

[1]*Centric Engineering Systems, Inc., 3393 Octavius Dr., Suite 201, Santa Clara, CA 95054, U.S.A.*
[2]*AeroSonix, Inc., 3393 Octavius Dr., Suite 201, Santa Clara, CA 95054, U.S.A.*
[3]*Nippon Sharyo, Ltd., 20 Honohara 2-Chome, Toyokawa-shi, Aichi-ken 442, Japan*

SUMMARY

Finite element and boundary element calculations are combined to predict the flow noise radiated from a 1/10th-scale model of an aerodynamic cover used around the pantograph on a train at 250 km h^{-1}. The solutions of the unsteady air flow over the cover and the resulting sound propagation are divided into two parts in order to keep the problem tractable. First the unsteady fluid flow is solved using large-eddy simulation (LES). The pressure histories on the cover are then used to predict the radiated sound, using a boundary element method to solve the Helmholtz equation. The result thus leans heavily on assumptions about the coupling of the two solutions, the propagation of sound in a disturbed medium and the efficacy of LES. The predicted sound pressure levels are compared with experimental measurements made in an anechoic wind tunnel. Ⓒ1997 by John Wiley & Sons, Ltd.

Int. J. Numer. Meth. Fluids, **24**: 1307–1319, 1997

No. of Figures: 8. No. of Tables: 2. No. of References: 20.

KEY WORDS: aeroacoustics; wind noise; time-dependent incompressible flows; large-eddy simulation; acoustic boundary elements; Helmholtz equation

1. BACKGROUND

It is generally acknowledged that public transportation systems that pass through densely populated areas should be as quiet as possible. High-speed trains may present noise problems because of their size, the speeds at which they operate and the proximity of homes. An important source of wind noise from trains is the pantograph system which is used on some trains to supply electrical power from overhead lines.[1]

Figure 1 shows the pantograph and cover system used in certain trains in Japan. The pantograph is designed to accommodate changes in line height as the train moves at high speed. Most pantographs look similar to the example shown and consist of a complex system of tubes and springs. This type of structure radiates a great deal of wind noise at high speed. To alleviate this problem, it is common to use an aerodynamic cover to deflect air over the pantograph. Reducing the local velocity around the

*Correspondence to: B. S. Holmes, Centric Engineering Systems, Inc., 3393 Octavius Dr., Suite 201, Santa Clara, CA 95054, U.S.A.

CCC 0271–2091/97/121307–13 $17.50

Received 17 July 1996
Revised 30 August 1996

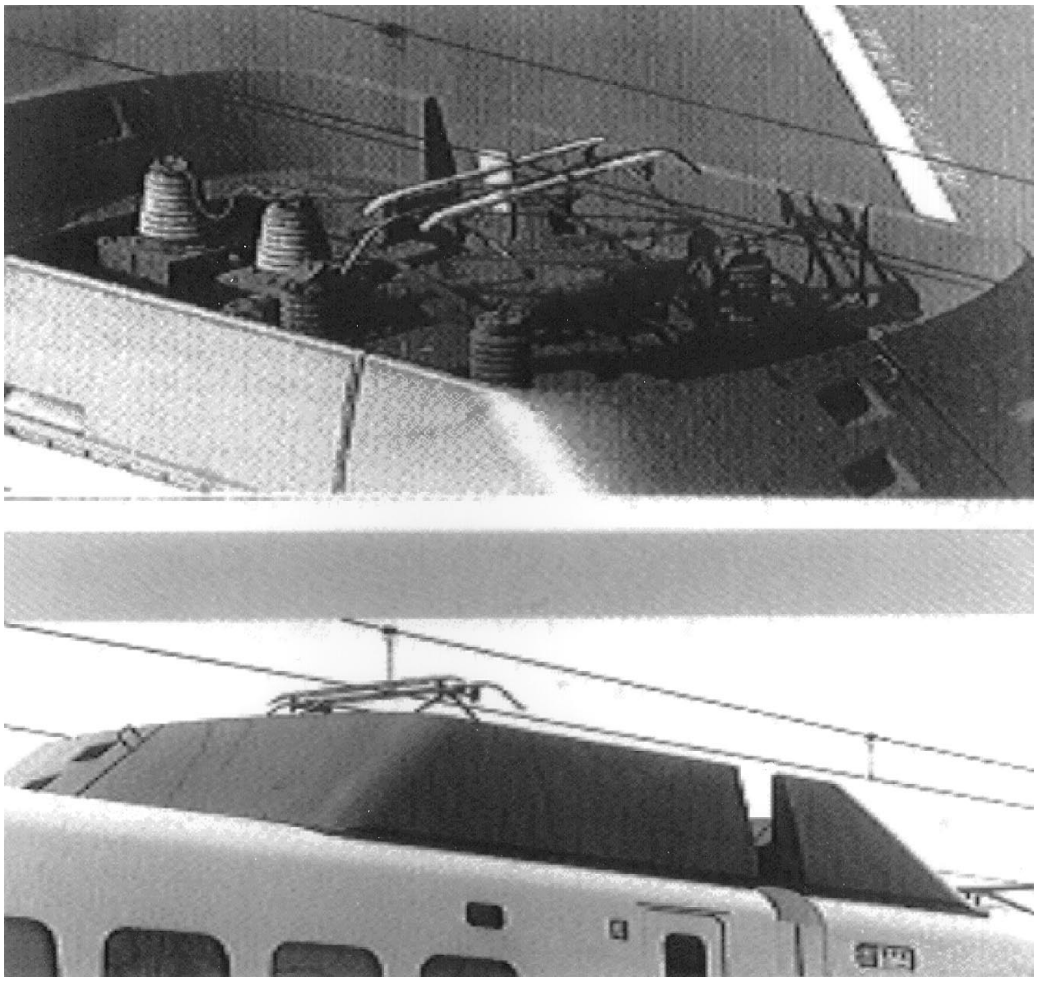

Figure 1. Pantograph with aerodynamic cover

pantograph dramatically reduces the wind noise from the pantograph, but the cover itself may radiate noise at different frequencies.

In this paper we predict the wind noise from a 1/10th-scale model pantograph cover and compare the results with data from experiments. The purpose of the analysis is both to study the efficacy of these large-scale calculations and to understand how the cover generates wind noise. The experiments used for comparison were performed on a 1/10th-scale model in air at a velocity of 70 m s^{-1}. Scaled experiments were used because of the difficulty of making acoustics measurements in a wind tunnel at full scale (the cover alone is about 7 m long).

Figure 2 shows a plan view of the 1/10th-scale model experiments which were performed in the test chamber of an anechoic wind tunnel. In the experiments, models of the cover and pantograph were placed on a flat table near the wind tunnel noizzle. The table surface replaces the curved roof of the train and the nozzle and table are located in a large acoustically treated chamber. Microphones were located at the level of the top of the cover at locations 1–6 as shown in Figure 2.

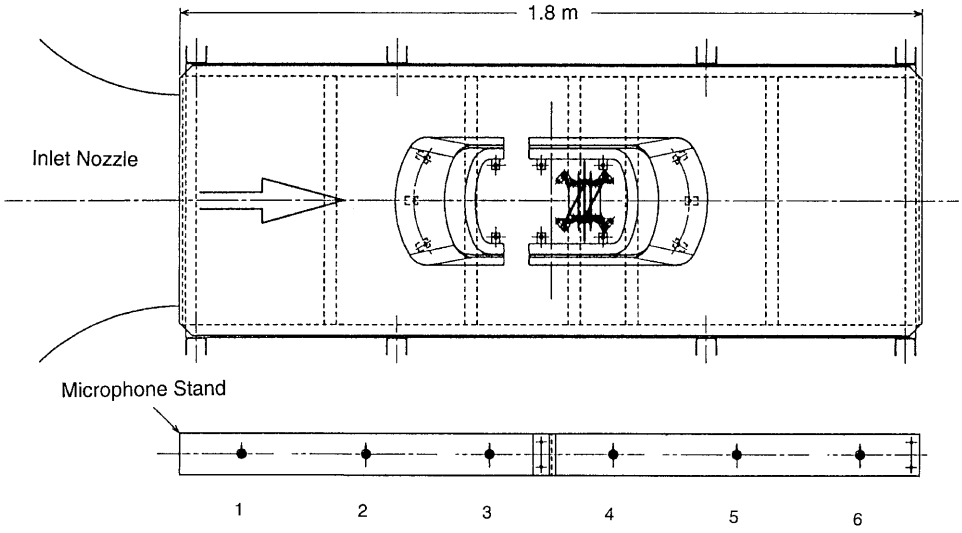

Figure 2. Plan view of wind tunnel experimental set-up

Experiments were run with four different model configurations as shown in Table I. By examining the sound measurements with different combinations of table, pantograph and cover, it is possible to show the relative contributions to wind noise from the cover and pantograph. This is best seen in Figure 3, which contrasts the sound pressure level (SPL, referenced to 2×10^{-5} Pa) frequency plots at microphone 3 (chosen as representative) for the four configurations in Table I. Each frame in Figure 3 shows the SPL in 1/3-octave bands from 4 Hz to 16 kHz. The last two bars on the right of each graph are the A-weighted and unweighted overall SPL.[2]

The first graph in Figure 3 is the SPL measured in a baseline test with only the support table for the model in the wind tunnel (Figure 3(a)). This test shows a significant noise level between 25 and 80 Hz. Comparison of the baseline data (Figure 3(a)) with SPL data for the case of a pantograph only (Figure 3(b)) shows that the scale model pantograph radiates sound in the frequency range from 500 to 16,000 Hz when no cover is used. At other frequencies below 100 Hz the SPL is at the levels of the baseline configuration, so that the noise generation by the pantograph cannot be determined. The addition of the streamlined cover effectively reduces the noise from the model pantograph at frequencies above 1000 Hz by deflecting the main air flow over the pantograph and thus reducing the local flow velocity (Figure 3(c)). Hence the cover is effective at reducing the high-pitched noise from the pantograph. However, the cover itself appears to produce increased noise at frequencies from 50 to 1000 Hz. This is seen by comparing Figures 3(b) and 3(c). Finally, the noise produced by the combination of the pantograph and cover and that produced by the cover alone were practically

Table I. Model test configurations

Configuration	Table	Pantograph	Cover
1. Baseline	Yes	No	No
2. Pantograph	Yes	Yes	No
3. Pantograph and cover	Yes	Yes	Yes
4. Cover only	Yes	No	Yes

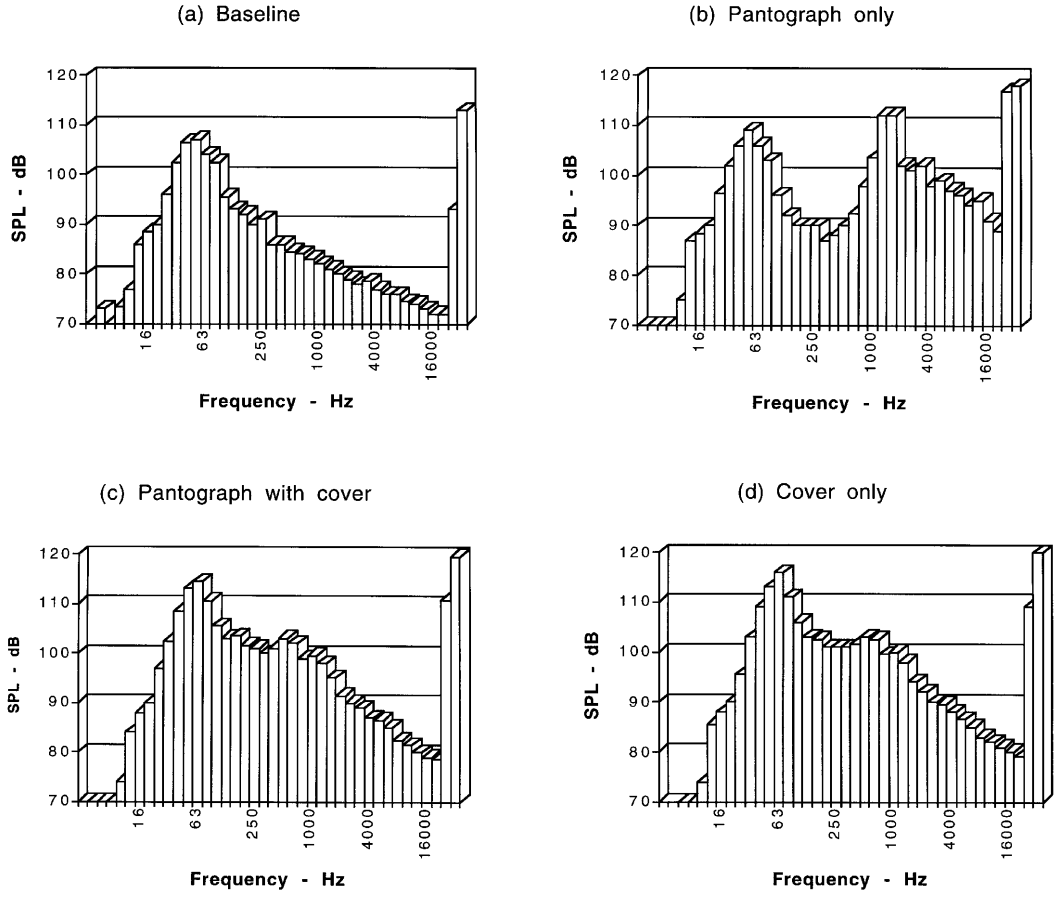

Figure 3. Sound pressure level data from microphone station 3

indistinguishable (Figures 3(c) and 3(d)). This suggests that the cover becomes the principal contributor to wind noise when it is used with a pantograph.

SPL spectra measured at the other five microphone locations were similar in shape to the measurements made at location 3. However, there was a significant variation in sound pressure level with location for all configurations. In particular, the microphones near the wind tunnel nozzle (locations 1 and 2) usually show higher overall SPL than those at location 3 and the microphones at locations 4–6 usually show lower overall SPL than those at location 3. The overall SPL varies from 111 to 121 dB for the case of pantograph cover only. The SPL for the $1/3$-octave band centred on 315 Hz varies from 101 to 88 dB. These are significant spatial variations and we will refer to these features of the data later when we make comparisons with experiments. We attribute these differences to noise from the blower and nozzle system and to jet noise from the mixing layer between the nozzle exhaust and the surrounding air. An additional effect is the advection of the sound in the high-speed flow.

On the basis of the observations made from the experiments, we decided to model the pantograph cover without the pantograph and focus on those design features in the cover that produce noise. This approach may lead to improved designs once the flow around the cover is better understood.

2. COMPUTATIONAL APPROACH

The problem of direct prediction of wind noise has been the subject of many recent numerical studies. Although it is appealing to attempt to solve for wind noise through direct solution of the compressible Navier–Stokes equations, this type of solution is virtually impossible for three-dimensional problems using existing computers. As pointed out by Tam,[3] the problems with such a direct approach arise because of the wide range of pressures in the fluid and the large fluid domain of interest. Pressure oscillations typically vary by three orders of magnitude from the noise source to the point of measurement, requiring very accurate numerical schemes. In addition, conflicts between the domain and mesh size requirements for the acoustics and fluid flow problems lead to further inefficiencies if both the sound generation and sound propagation problems are solved together. For example, the sound generated by the pantograph cover on a full-scale train is governed by the flow within a few metres of the cover, while it may be desired to calculate the sound levels 500 m away from the cover.

The general approach pioneered by others[4–6] to resolve these issues is to divide the problem into two parts: a flow calculation to determine the unsteady fluid flow generating the sound and an acoustics calculation to determine the sound propagation. This kind of subdivision is suggested by the work of Lighthill[7] and Curle,[8] who showed that the Navier–Stokes equations could be reduced to an inhomogeneous wave equation if certain forcing terms are retained on the right-hand side. If a solution for the unsteady flow can be developed (even using the incompressible Navier–Stokes equations), the calculated pressures and changes in momentum may be used to predict the sound generated. Implicit in this approach are several assumptions regarding the energy terms in the equations,[7] but, more importantly, it is assumed that the flow is not influenced by the sound propagation and the problems can be solved sequentially. Also, it is assumed that the sound propagates in a fixed medium, i.e. the effect of the motion of the medium on the sound propagation can be neglected. The validity of this assumption becomes more suspect as the mean flow velocity increases. The calculations described here are for a Mach number of about 0·21 and could be considered a severe test of the method.

A final issue is the method used to solve the wave equation in the fictitious fixed surrounding medium. Lighthill and Curle derived exact integrals to predict sound pressure histories. Rather than use these relations here, we chose to solve for the acoustic field around the cover and at the microphone locations using a boundary element acoustics solver. Thus prediction of the noise generated from the pantograph cover was accomplished through two separate numerical calculations. The first is a calculation of the unsteady fluid flow over the model to predict the pressure fluctuations on the model surface. This calculation was completed using the SPECTRUM^{TM} solver.[9] The second calculation is the prediction of the sound radiated from the surface as a result of the fluctuating pressure. This was done using the RAYON^{TM} acoustics code.[10]

3. FLOW COMPUTATIONS

We solved the incompressible Navier–Stokes equations using a second-order- accurate finite element method based on the Galerkin least squares formulation.[11] The linear equations were solved with generalized minimum residual (GMRES) and conjugate gradient (CG) linear solvers in a ‘segregated’ solution strategy where each non-linear iteration consists of two ‘staggers’ or phases. In this strategy the consistent left-hand side (LHS) of the continuity and momentum equations is replaced with an approximate LHS that has better conditioning. In the first stagger the momentum equation is solved for velocity (with the pressure held fixed) using GMRES. In the second stagger a symmetric system is formed from the continuity equation, the pressure gradient term from the momentum equations and a

diagonal approximation of the remaining terms in the momentum equation. Four non-linear iterations are taken within each time step. This system is advanced in time using the Hilber–Hughes–Taylor (HHT) algorithm.[12] The HHT parameters were chosen to maintain second-order accuracy in time and a constant time step was chosen corresponding to a Courant–Friedrichs–Lewy (CFL) number of about 15.

We used Smagorinsky's large-eddy simulation (LES) turbulence model.[13] In this model the *ij*-component of the subgrid-scale Reynolds stress tensor is related to the large-scale strain rate by

$$\overline{u_i u_j} = \nu_T \bar{S}_{ij} = \tfrac{1}{2}\nu_T \left(\frac{\partial \bar{u}_i}{\partial x_j} + \frac{\partial \bar{u}_j}{\partial x_i} \right),$$

where

$$\nu_T = (C_s \Delta)^2 (\bar{S}_{ij} \bar{S}_{ij})^{1/2}$$

and Δ is the length scale associated with the grid. In our implementation of the model the length scale Δ is taken to be the cube root of the element volume. Thus the model captures the large eddies in the flow while adjusting the local fluid viscosity to model the effects of turbulence scales smaller than the grid size.

The flow calculations focus on the separated unsteady flow over the pantograph cover. These calculations differ from other examples of unsteady flow calculations around trains found in the literature which have dealt with the transients associated with passing trains or tunnel entry.[14,15]

Two different meshes were used in the flow computations. The first mesh was relatively coarse, consisting of 86,064 hexahedral elements and 92,545 nodes. A surface wireframe of this mesh is shown in Figure 4(a). The second mesh was constructed by dividing each element of the coarse mesh into eight smaller elements, for a total of 688,512 hexahedral elements and 714,161 nodes, as shown in Figure 4(b).

The flow simulations were initiated by running the coarse mesh from an impulsive start, using a dissipative version of the HHT algorithm with variable time step size, until a quasi-periodic vortex-shedding pattern was established. This took approximately 320 time steps. The simulation of the coarse mesh was continued for an additional 2048 time steps at a constant time step size of 5×10^{-6} s, using a time-accurate version of the HHT algorithm with four non-linear iterations per time step, in which detailed pressure histories were collected at *all nodes* on the cover and base surfaces.

A second transient solution was obtained with the fine mesh. Initial conditions derived from the flow solution compared on the coarse mesh at the end of the initial 320 time steps were mapped onto the fine mesh and the problem was run for an additional 512 time steps at a constant time step size of 5×10^{-6} s. Again a time-accurate version of the HHT algorithm with four non-linear iterations per time step was used. However, detailed pressure histories were collected *only at those surface nodes whose co-ordinates correspond to the location of a coarse mesh node*, allowing us to employ the same surface mesh for all acoustic computations. It was anticipated that this solution should better resolve the finer flow structures and give us a better prediction of the aeroacoustic noise at higher frequencies.

Before proceeding with a discussion of the results, it is worth examining the effect of time step size and overall sampling interval in determining the frequencies that we can expect to resolve in these calculations. The maximum frequency that can be resolved is the Nyquist frequency, determined by the sampling interval Δt, i.e.

$$f_{\max} = 1/2\Delta t.$$

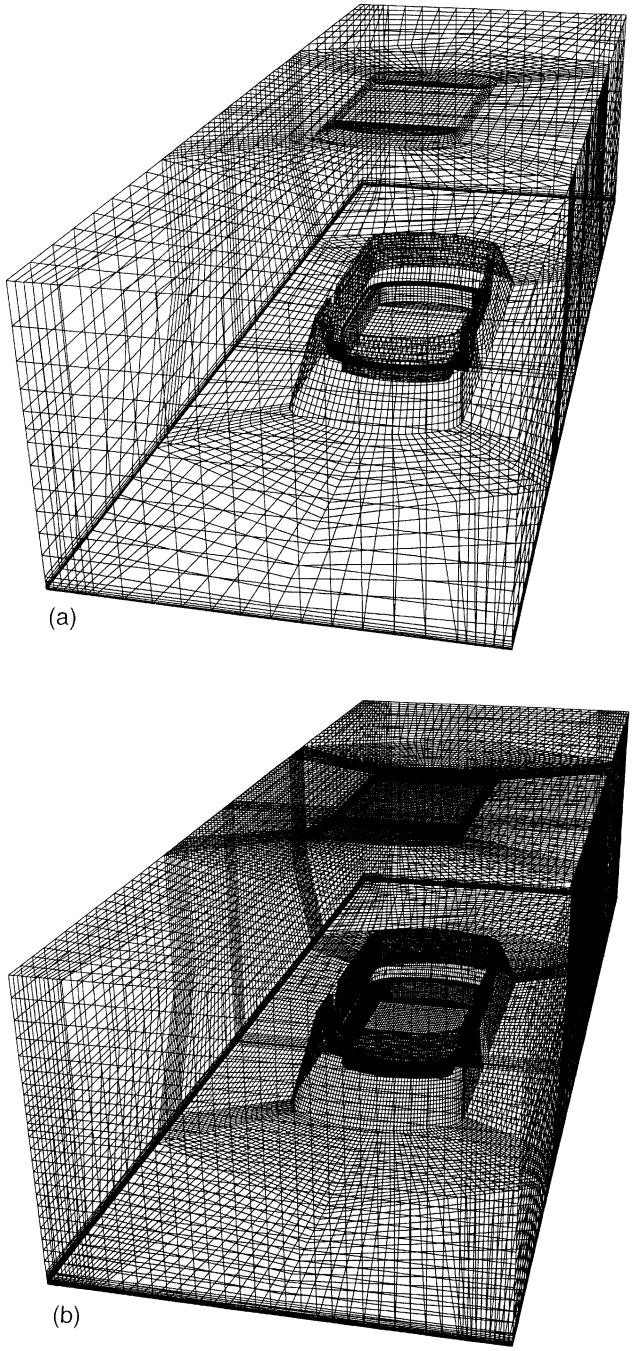

Figure 4. Surface wireframes of (a) coarse and (b) fine meshes

In practice the Nyquist frequency is several times higher than the frequencies which are accurately resolved in the fluid flow calculations for a given degree of mesh refinement and time step size. Instead we propose to estimate the highest resolved frequency (f_r) as that which is given by the formula

$$f_r = 0{\cdot}1 U_\infty / h,$$

where U_∞ is the freestream velocity and h is some average element dimension in the region where turbulent flow noise is generated. Thus the constant 0·1 has the appearance of a Strouhal number for the mesh.

The lowest frequency that we can expect to resolve (f_{min}), other than the constant component of the signal, is one over the sampling interval:

$$f_{min} = 1/T = 1/\sum \Delta t.$$

Again in practice we would like to have an overall sampling interval that spans ten or more complete periods at the lowest frequency of interest in order to more accurately average the physical behaviour at these low frequencies. Table II gives the values of the various frequency limits for the coarse and fine meshes used in this problem.

All transient flow solutions were obtained using parallel processing on a IBM SP2. The coarse mesh solution was obtained using a four-subdomain decomposition on six processors of the SP2. The solution averaged 4·8 min per time step for a total wall time of approximately 166 h. The fine mesh problem was run in parallel using a decomposition of 32 subdomains on 34 processors. The solution averaged 8 min per time step for a total wall time of approximately 68 h.

Visualization of the results from both transient flow computations showed that the pantograph cover effectively deflects the high-speed flow over the pantograph location, creating pockets of slower unsteady mixing flow both within the pantograph cover and downstream from it. A typical visualization of the transient flow solution computed on the fine mesh at a particular instant in time is shown in Plate 1(a). Pressure contours are plotted on the surface of the pantograph cover and base and fluid velocity vectors are shown for a rectangular slice probe located at the sagittal plane of the model. We can see an almost steady pattern of high pressures surrounding the stagnation point at the front of the cover. Note how the velocity vectors within the pantograph cover and downstream from it exhibit the swirling patterns characteristic of transverse vorticity in the flow. The three-dimensional nature of these flow structures can be seen more clearly by adding pressure isosurfaces to the visualized scene as shown in Plate 1(b). The green cloud-like formations shown in this Plate are three-dimensional pressure isosurfaces enclosing the low- pressure cores of transverse vortices which are being shed from the leading edge of the pantograph cover in a quasi-periodic manner. It is interesting to note the visible asymmetry of these large flow structures, suggesting that some degree of streamwise vorticity and side-to-side variation is also present in this flow. These vortices are convected downstream by the flow and impinge on the back of the pantograph cover, giving rise to

Table II. Expected frequency limits for coarse and fine mesh solutions

	Coarse mesh	Fine mesh
f_{max} (Hz)	10000	10000
f_r (Hz)	350	700
f_{min} (Hz)	10	40

very unsteady (and often asymmetric) pressure patterns at that location, as seen in Plate 1(a). This appears to be the prevalent mechanism of aeroacoustic noise generation. Note also the low-pressure pockets attached to the corners of the pantograph cover, associated with flow separation at these locations. These are very unsteady flow features which may also contribute to aeroacoustic noise generation.

Further insights may be gained by probing the flow field with combs of streamlines. Plate 2 shows the streamline combs emanating from three different line probes placed horizontally across the flow at different heights from the base. The lowermost comb (yellow streamlines) begins almost flush with the top of the base and is found to roll up into a delicate pair of vortex braids at the front of the pantograph cover (this is essentially a three-dimensional counterpart to the classical foward-facing step solution). We shall see that these vortex braids also appear to contribute to aeroacoustic sound generation at certain frequencies. The next comb (pink streamlines) is observed to dip within the pantograph cover, where the individual streamlines follow erratic paths before spilling over the back into the wake of the pantograph cover. Finally, the uppermost comb (blue streamlines) is effectively diverted over the pantograph cover, with the individual streamlines following gently curved paths around the cover before beginning to mix with the pink streamlines in the turbulent wake of the pantograph cover.

4. ACOUSTIC CALCULATIONS

The acoustic computations were based on a special implementation of the boundary element method (BEM). This implementation is part of a general mixed FEM–BEM variational formulation used in RAYON^{TM} for modelling the elastoacoustic response of complex 3D structures coupled to one or several acoustic fluid domains and subject to time-harmonic mechanical and/or acoustic loads. The details of this formulation are discussed elsewhere,[16,17] and will not be repeated here. However, a brief summary is provided in the Appendix.

As mentioned in Section 2, the results of the unsteady flow calculations were used to predict the noise radiated from the base and cover at frequencies between 50 and 2000 Hz. The time domain surface pressure fluctuations were transformed into the frequency domain using a standard FFT algorithm. Although the frequency content of the transformed data covers the theoretical range of 50–2000 Hz, the practical range of validity is significantly lower owing to the CFD considerations presented in the preceding section.

Qualitative examination of these harmonic pressure distributions can yield significant insight into the character of the acoustic solution even before the actual SPL is computed at each microphone location. In particular, one can argue that the bulk of the predicted sound generation is radiated from the surfaces on the back of the cover and the surface of the table in the wake of the cover. Plate 3 illustrates this point with data taken from the calculation with the fine mesh. Here surface pressure amplitude at a frequency of 390·6 Hz is plotted as colour contours on the cover and table. This is essentially a single component of the boundary condition used as input to the acoustics solver. The Plate shows that that highest input amplitudes at this frequency are concentrated on the inside of the cover and in two trails on the left and right sides of the cover wake. This plot also shows an interesting artefact of the calculation length. We would expect that over a long period of time this plot would be symmetric about the sagittal plane. The fact that there are some asymmetries in the plot is probably a result of the calculation length; at a frequency of 390·6 Hz there are approximately 10 complete cycles in the calculation.

Quantitative acoustics results are presented in Figure 5, where the predicted sound pressure level data were compared with the actual microphone readings; the darker bars are the analysis results and

the lighter bars are the experimental results. The results obtained with the coarse mesh are presented in Figure 5(a) and those obtained with the fine mesh in Figure 5(b).

Referring first to Figure 5(a), we observe that the analysis overpredicts the SPL at frequencies of 100–200 Hz and underpredicts the SPL at frequencies above 400 Hz. It is difficult to make a quantitative comparison between analysis and experiment below 50 Hz owing to the background noise at these frequencies noted earlier.

A similar comparison is made in Figure 5(b) using the results obtained with the fine mesh. In this case, better agreement is found at all frequencies. However, above 500 Hz the predicted SPL still falls off rapidly.

It should be noted that the variation in SPL with microphone location was not as pronounced in the analysis results as in the experimental measurements. This may be due to the proximity of the wind tunnel nozzle in the experiments, noise from the mixing zone at the edges of the nozzle and the

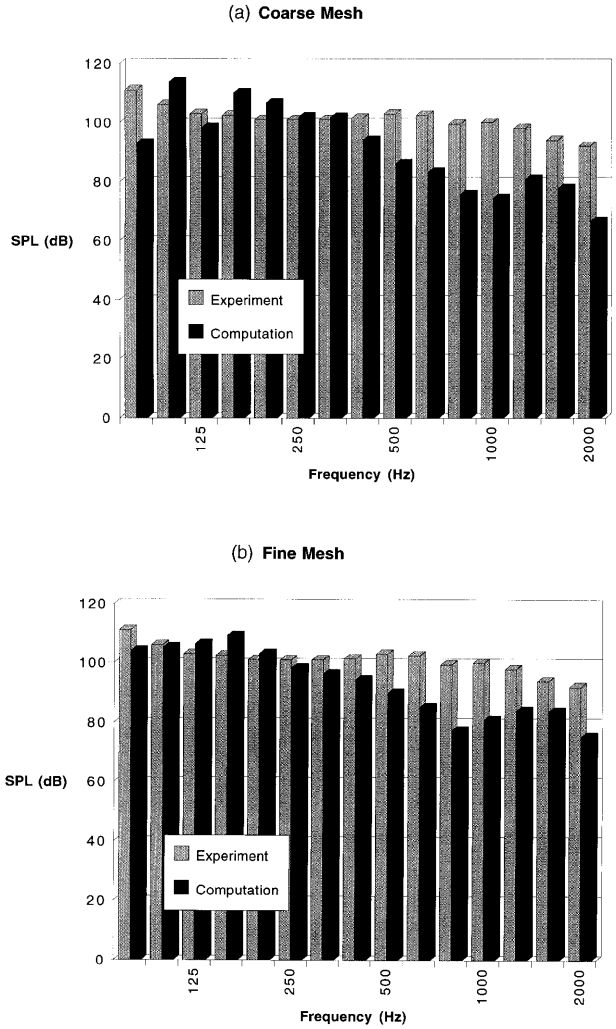

Figure 5. Comparisons of predicted SPL with measurement data

advection of the sound field. It is difficult to quantify these effects. Most studies of the noise from nozzles have concentrated on Mach numbers near 1 or higher. However, Mitchell *et al*.[18] and Soh[19] have studied the far-field noise from jets at Mach numbers of 0·4 and 0·6 respectively and have shown significant directivity in the radiated sound. In any case the agreement illustrated here is typical for all microphone locations.

Generally good agreement was obtained between the analysis and the experiments at the other microphone locations. Significantly, the predicted overall sound pressure level obtained by summing the contributions over frequencies between 125 and 700 Hz was within 4 dB of that measured for three of the six microphones. The maximum error in overall SPL was 8 dB (at location 3).

5. CONCLUSION

A series of calculations was used to predict the wind noise from a pantograph. The approach used was to divide the calculation into an unsteady incompressible flow calculation and an acoustic wave propagation calculation. Two fluid flow problems corresponding to two levels of mesh refinement were solved on a multiprocessor computer. The corresponding acoustics solutions were obtained on a workstation. The predicted sound pressure levels were compared with microphone measurements. General agreement was found between the analysis and experiment, although significant differences were found at some frequencies.

Examination of the results of the calculations revealed several important features of the flow field and the mechanisms of sound generation. One of the most important observations was that the pantograph cover tended to shed a series of large transverse vortices from its front edge which were convected downstream and impinged on the back edge of the cover. This interaction seemed to generate much of the predicted sound. From this we might conclude that changes in cover geometry may reduce radiated sound by reducing the interaction between the vortices and the rear of the cover.

The work described here is an application of several modern computational aeroacoustics techniques to a large-scale industrial problem with complex geometry. One of the important contributions of the analysis appears to be the increased understanding of the flow features that lead to noise. It would appear that this type of analysis is most useful in providing insight into the mechanisms of aeroacoustic noise generation, suggesting geometry changes which might be useful in reducing noise.

Although the initial results appear promising, further improvements are needed. In particular, finer resolution of the flow is needed in order to resolve higher frequencies. The large-eddy simulation model used here is known to be deficient in solving some flow problems and may not give similar results when applied to other wind noise problems.[20]

APPENDIX: NOTES ON ACOUSTIC COMPUTATION

The mixed FEM–BEM variational formulation implemented in RAYON^{TM} is capable of solving for the linear elastoacoustic response of complex 3D structures coupled to one or more acoustic fluid domains and subject to time- harmonic mechanical and/or acoustic loads. The structures are represented by the classical FEM discretization. In RAYON^{TM} all acoustic fluids are considered perfect and barotropic. The internal fluid domains (cavities) can be represented by either an acoustic FEM or BEM discretization. The external acoustic fluids are always represented by a BEM discretization, so that the Sommerfield radiation condition (outgoing waves only, far away from the sources) can be satisfied exactly.

In the simplified problem solved here, RAYON^{TM} was used to solve for sound propagation outside the train. However, it could also be used to solve for the response of the train structure coupled

simultaneously with the air inside and outside the cars. Indeed, as a continuation of the work reported here, the authors are currently carrying out predictions of the noise generated by the flow over the train roof and pantograph shroud structure, and its transmission to the train car interior, when the train is passing through a tunnel. Results from this work will be presented in a future publication.

For the present problem the pressure in the external fluid is governed by the Helmholtz equation

$$\Delta P + k^2 P = 0,$$

where $k = \omega/c$ is the wave number, ω is the radian frequency and c is the speed of sound in this fluid. The boundary conditions for this simplified problem are $P = P$ on the upper surfaces of the pantograph shroud and supporting table, which are exposed to the flow, $\partial P/\partial n = 0$ on the lower surface of the supporting table and $\lim r|\partial P/\partial r - ikP| = 0$ as $r \to \infty$ (Sommerfeld radiation condition).

In order to derive a general integral representation of the acoustic pressure which is valid for external as well as internal problems, the Helmholtz equation is rewritten using distribution theory as

$$(\Delta + k^2)P = \sigma\delta_S + \partial(\mu\delta_S)/\partial n,$$

where μ and σ are respectively the jump in the acoustic pressure and its normal derivative across the integration surface S and δ_S is a Dirac distribution applied at S.

Further use of the properties of convolution and the Dirac distribution yields the following expression for the acoustic pressure at any point M outside the integration surfaces (Q is a running point on the integration surface):

$$P(M) = \int_S (\mu_Q \partial g(M,Q)/\partial n_Q - \sigma_Q g(M,Q)) \mathrm{d}S_Q,$$

where $g(M, Q)$ is the free space Green function solution of the inhomogeneous Helmholtz equation satisfying the Sommerfeld radiation condition. This expression is the starting point for the variational formulation and BEM discretization of the external problem.

Notice that when the point M lies in the integration surface, the above integral is singular and has to be evaluated in the sense of Cauchy's principal value. Furthermore, if the integration surface represents an elastic fluid–structure interface, a similar integral can be derived for the normal displacement. This integral has a second-order singularity and has to be evaluated in the sense of Hadamard's finite part. One advantage of the BEM variational formulation used in RAYON^{TM} is avoiding the explicit evaluation of these hypersingular integrals while still yielding a symmetric system of equations which can be solved using fast algorithms developed for the classical FEM.[16,17]

REFERENCES

1. K. Iwamoto and A. Higashi, 'Some consideration toward reducing aerodynamic noise on pantograph', *Jpn. Railway Eng.*, **122**, 1– 4 (1993).
2. A. Pierce, *Acoustics*, Acoustical Society of America, 1989, pp. 60- -68.
3. C. Tam, 'Computational aeroacoustics: issues and methods', *AIAA J.*, **33**, 1788–1796 (1995).
4. C. Kato, A. Iida, Y. Takano, H. Fujita and M. Ikegawa, 'Numerical prediction of aerodynamic noise from low Mach number turbulent wake', *AIAA Paper 93-1045*, 1993.
5. J. C. Hardin and S. L. Lamkin, 'Aeroacoustic computation of cylinder wake flow', *AIAA J.*, **22**, 51–57 (1984).
6. S. Haruna, M. Hashiguchi, I. Kamimoto and K. Kuwahara, 'Numerical study of aerodynamic noise radiated from a three-dimensional wing', *SAE Paper 920341*, 1992.
7. M. J. Lighthill, 'On sound generated aerodynamically: I. General theory', *Proc. R. Soc. A*, **211**, 564–587 (1951).
8. N. Curle, 'The influence of solid boundaries upon aerodynamic sound', *Proc. R. Soc. A*, **231**, 505–514 (1955).
9. *Parallel Spectrum Solver^{TM} User Guide*, Release 2.0 (mp810), Centric Engineering Systems, Inc., 1995.
10. *Rayon^{TM} User's Manual*, Version 4.0, STRACO S.A., 1994.

11. T. J. R. Hughes, L. P. Franca and G. M. Gilbert, 'A new finite element formulation for computational fluid dynamics: VIII. The Galerkin/least-squares method for advective–diffusive equations', *Comput. Methods Appl. Mech. Eng.*, **73**, 173–189 (1989).
12. H. M. Hilber, T. J. R. Hughes and R. L. Taylor, 'Improved numerical dissipation for time integration algorithms in structural dynamics', *Earthquake Eng. Struct. Dyn.*, **5**, 283–292 (1977).
13. J. Smagorinsky, 'General circulation experiments with the primitive equations: I. The basic experiment', *Mon. Weather Rev.*, **91**, 99–164 (1963).
14. V. Kalro and T. E. Tezduyar, 'Parallel finite element computation of 3D incompressible flows on MPPs', in *Solution Techniques of Large- Scale CFD Problems*, John Wiley, New York, 1995.
15. S. Aïta, A. Tabbal, E. Mestreau, N. Montmayeur, F. Masbernat, Y. F. Wolfhugel and J. C. Dumas, 'CFD aerodynamics of the French high speed train', *SAE Paper 920343*, 1992.
16. M. A. Hamdi, 'Une formulation variationnelle par équations intégrales pour la résolution de l'équation de Helmholtz avec des conditions aux limites mixtes', *C. R. Acad. Sci. Paris II*, **292**, 17–20 (1981).
17. J. Ben Mariem and M. A. Hamdi, 'A new boundary finite element method for fluid–structure interaction problems', *Int. J. numer. methods eng.*, **24**, 1251–1267 (1987).
18. B. E. Mitchell, S. K. Lele and P. Moin, 'Direct computation of the sound generated by vortex pairing in an axisymmetric jet', *AIAA Paper 95-0504*, 1995.
19. W. Y. Soh, 'Unsteady jet flow computation: towards noise prediction', *AIAA Paper 94-0138*, 1994.
20. J. H. Ferziger, 'Subgrid-scale modeling', in *Large Eddy Simulation of Complex Engineering and Geophysical Flows*, Cambridge University Press, Cambridge, 1993, pp. 37–54.

